Journal of Colloid and Interface Science 405 (2013) 269–277

Contents lists available at SciVerse ScienceDirect

Journal of Colloid and Interface Science

www.elsevier.com/locate/jcis

Forces acting on dielectric colloidal spheres at a water/nonpolar fluid interface in an external electric field. 2. Charged particles

Krassimir D. Danov, Peter A. Kralchevsky *

Department of Chemical Engineering, Faculty of Chemistry & Pharmacy, Sofia University, 1164 Sofia, Bulgaria

ARTICLE INFO

Article history:
Received 18 March 2013
Accepted 2 May 2013
Available online 18 May 2013

Keywords:
Charged particles at a liquid interface
Non-densely packed interfacial colloid crystals
Particle arrays in external electric field
Contact angle
Electrodipping force
Electrostatic repulsion between floating particles

ABSTRACT

Here, we calculate the electric forces acting on charged dielectric colloidal particles, which are attached to the interface between a nonpolar fluid (air and oil) and water in the presence of applied uniform external electric field, E_0, directed normal to the interface. Electric charges are present on the particle–nonpolar fluid interface. The solution to the problem represents a superposition of the solutions of two simpler problems: (i) charged particle in the absence of external field and (ii) uncharged particle in the presence of external field. Because the external field can be directed upward or downward, it enhances or opposes the effect of the particle surface charges. As a result, the vertical (electrodipping) force vs. E_0 may have a maximum or minimum and can be positive or negative depending on the particle contact angle and dielectric constant. In contrast, the lateral electric force between two identical charged floating particles is always positive (repulsive), but it can vary by many orders of magnitude with E_0. This is because at a certain value of E_0, the net dipolar moment of the particle becomes zero. Then, the interparticle force is governed by the octupolar moment, which leads to a much weaker and short-range repulsion. In the vicinity of this special value of E_0, the interparticle repulsion is very sensitive to the variations in the external field. These effects can be used for a fine control of the lattice spacing in non-densely packed interfacial colloidal crystals of regular hexagonal packing for producing lithographic masks with various applications in nanotechnology.

1. Introduction

The aim of the present study is to calculate the electrostatic forces acting on charged dielectric particles attached to a water–nonpolar fluid interface in the presence of external electric field, E_0, directed normal to the interface. The solution to this problem can be found by combining the solutions of two simpler problems: (i) charged particles without external field [1] and (ii) uncharged particles in external field [2]. In the latter case, the particle becomes a source of electric field because of its polarization by the external field. Our final goal is to calculate the normal (electrodipping) force $F^{(n)}$ acting on each separate particle, and the electrostatic interaction force F_{12} between two floating particles, as well as the dependencies of $F^{(n)}$ and F_{12} on the particle contact angle and dielectric constant. The value of $F^{(n)}$ includes a contribution from an integrable singularity at the contact line on the particle surface. To accurately take into account this contribution, in preceding studies [1,2], we solved the respective electrostatic boundary problem analytically, by using the Mehler–Fock integral transform.

The experiment shows that by varying the strength of the applied external electric field, one can control the electrostatic and capillary interactions between particles collected at an interface, and the distances between the particles in a non-densely packed two-dimensional colloid array formed at a liquid interface [3–8]. Such arrays have been obtained by spreading of charged colloidal particles on a liquid interface [9–16]. They have found applications for the creation of lithographic masks in the production of periodic nano-structures, e.g., antireflection coatings, microlens arrays, etc. [16–22].

The normal force acting on a floating colloidal particle creates an interfacial deformation (capillary meniscus) around the particle. The overlap of such menisci gives rise to capillary attraction between the particles [23–28]. The attractive capillary force can be due also to out-of-plane undulations of the contact line because of surface roughness or to non-spherical shape of the particle, the so-called interactions between capillary multipoles [29–36]. The interplay of electrostatic repulsion and capillary attraction affects the interparticle spacing in the non-densely packed interfacial colloid arrays and the surface pressure in such particulate monolayers [31,32,37].

As in Ref. [1], here we assume that charges of uniform surface density σ_{pn} are located at the particle–nonpolar fluid (air and oil) interface. Experimentally, this was observed with micrometer-sized and bigger particles [9–11,38,39]. Indication for the predominant effect of σ_{pn} is the lack of dependence of particle interactions

* Corresponding author. Fax: +359 2 9625643.
E-mail address: pk@lcpe.uni-sofia.bg (P.A. Kralchevsky).

0021-9797/$ - see front matter © 2013 Elsevier Inc. All rights reserved.
http://dx.doi.org/10.1016/j.jcis.2013.05.015

and of their conformation at the interface on the concentration of electrolyte in the aqueous phase [11,38]. This situation is typical for particles of radius R, which is much greater than the Debye screening length in the water phase, i.e., $\kappa R \gg 1$. In such a case, the electrostatic interactions across the water phase are negligible and only the electric effects in the nonpolar fluid and inside the dielectric particle are essential [38]. For smaller particles ($\kappa R \leqslant 1$), the interaction across the aqueous phase can become significant [40–43].

Here, we first combine the solutions of the problems for a charged particle without external field [1] and for an uncharged particle in external field [2] to obtain the electric field around a charged particle in external field (Section 2). Next, a general expression for the normal force $F^{(n)}$ is derived and applied to the considered system. The magnitude and direction of this force (dipping or pulling) depending on the applied external field E_0 are investigated (Section 3). Further, the lateral electric force F_{12} between two particles at the liquid interface is calculated for not-too-small interparticle distances. The effects of the particle contact angle, dielectric constant, and E_0 on F_{12} are also investigated. For reader's convenience, the respective force coefficients are tabulated in Appendix A. Thus, the reader could simply calculate $F^{(n)}$ and F_{12} with the help of a four-point interpolation formula, instead of repeating the time-consuming numerical computations.

2. Physical system and basic equations

2.1. Combination of the solutions for charged particle without external field and uncharged particle in external field

Here, we consider a spherical particle of radius R, which is attached to a flat interface between water and a nonpolar fluid (oil, air, etc.); see Fig. 1. Surface charges of uniform density σ_{pn} are located at the particle–nonpolar fluid boundary, S_{pn}. A uniform external electric field is applied perpendicular to the fluid interface, with a vertical projection E_0. The dielectric constants of the water, nonpolar fluid, and particle are denoted ε_w, ε_n, and ε_p, respectively.

As in Refs. [1,2], we assume that $\varepsilon_w \gg \varepsilon_p, \varepsilon_n$. For this reason, the electric field in the nonpolar fluid and in the dielectric particle practically does not penetrate into the water phase; see, for example, the conventional problem for the image force [44] and for a charged hydrophobic particle near the oil–water interface [45]. Experimentally, the non-penetration of the field into water is manifested as independence of the configuration of the adsorbed particles on the electrolyte concentration in the aqueous phase [11,38]. This is fulfilled in the case $R \gg \kappa^{-1}$, where κ is the Debye screening parameter. However, for smaller particles, for which R is comparable with κ^{-1}, the effect of the electrostatic field in the water becomes material [38].

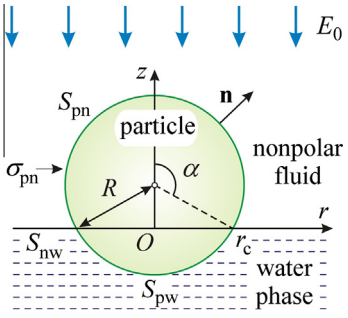

Fig. 1. Sketch of a charged spherical colloidal particle attached to the water–nonpolar fluid interface, S_{nw}. The particle–nonpolar fluid and particle–water interfaces are denoted S_{pn} and S_{pw}, respectively; $\mathbf{n}$ is the outer unit normal to S_{pn}; E_0 is a uniform external field. The surface charges of density σ_{pn} are located at S_{pn}.

In zero-order approximation, we assume that the water–nonpolar fluid interface is planar. The position of the particle at the interface is defined by the central angle, α, which coincides with the three-phase contact angle if the water–nonpolar fluid interface is flat (Fig. 1). In particular, $\alpha < 90°$ for hydrophilic particle and $\alpha > 90°$ for hydrophobic particle. The three-phase contact line is a circumference of radius r_c.

The potential of the electric field, φ_p inside the particle and φ_n in the nonpolar fluid, obeys the Laplace equation,

$$\nabla^2 \varphi_k = 0, \quad k = p, n, \tag{2.1}$$

where ∇^2 is the Laplace operator. Having assumed non-penetration of the electric field into water, the role of the water is to keep the electric potential constant at the boundaries S_{nw} and S_{pw} (Fig. 1). Because the latter constant can be set zero, we obtain the following two boundary conditions:

$$\varphi_p = 0 \text{ at } S_{pw} \quad \text{and} \quad \varphi_n = 0 \text{ at } S_{nw}. \tag{2.2}$$

At the third interface, S_{pn}, we impose the standard boundary conditions for continuity of the electric potential and the relation between the normal electric-field components:

$$\varphi_n = \varphi_p \quad \text{and} \quad \mathbf{n} \cdot (\varepsilon_p \nabla \varphi_p - \varepsilon_n \nabla \varphi_n) = 4\pi\sigma_{pn} \quad \text{at} \quad S_{pn}, \tag{2.3}$$

where ∇ is the del operator and $\mathbf{n}$ is the outer unit normal to the particle surface, S_{pn} (Fig. 1). In the nonpolar fluid at large distances from the particle, the external electric field is $\mathbf{E}_0 = -E_0\mathbf{e}_z$, where $\mathbf{e}_z$ is the unit vector of the vertical axis z (Fig. 1). Then, the electric potential should have the following asymptotic form:

$$\varphi_n \to E_0 z \quad \text{far from the particle.} \tag{2.4}$$

Because of the linearity of the considered boundary problem, Eqs. (2.1)–(2.4), the solution can be presented as a superposition:

$$\varphi_n = \varphi_{\sigma,n} + \varphi_{E,n} \quad \text{and} \quad \varphi_p = \varphi_{\sigma,p} + \varphi_{E,p}, \tag{2.5}$$

where $\varphi_{\sigma,n}$ and $\varphi_{\sigma,p}$ are the solutions of the problem for a charged particle without external field, which has been considered in Ref. [1], and $\varphi_{E,n}$ and $\varphi_{E,p}$ are the solutions of the problem for an uncharged particle with applied external field, which has been considered in Ref. [2].

2.2. Basic expressions for the electric field

Here, we briefly summarize the basic expressions, which will be used to calculate the normal (electrodipping) force acting on a single floating particle and the lateral force of electrostatic interaction between two such particles. As demonstrated in Refs. [1,2], for this goal we need to know the vertical component of the electric field, $E_z = -\mathbf{e}_z \cdot \nabla\varphi_n$, at the flat interface between the nonpolar fluid and water, S_{nw}, where $z = 0$; $\mathbf{e}_z$ is the unit vector of the z-axis (Fig. 1). In view of Eq. (2.5), we can write:

$$E_z = E_{\sigma,z} + E_{E,z}. \tag{2.6}$$

where $E_{\sigma,z} = -\mathbf{e}_z \cdot \nabla\varphi_{\sigma,n}$ and $E_{E,z} = -\mathbf{e}_z \cdot \nabla\varphi_{E,n}$. The fact that $E_{\sigma,z}$ and $E_{E,z}$ at S_{nw} have been already found in Refs. [1,2], considerably simplifies our task in the present study. More specifically, summarizing Eqs. (3.22) and (3.23) in Ref. [1], and Eq. (3.20) in Ref. [2], we obtain:

$$E_{\sigma,z} = -\frac{4\pi}{\varepsilon_n}\sigma_{pn}\frac{x_1^3 J_\sigma}{(1-x_1)^{1-\nu}} \quad \text{and} \quad E_{E,z} = -E_0 - E_0\frac{x_1^3 J_E}{(1-x_1)^{1-\nu}}, \tag{2.7}$$

$$J_j(x_1, \alpha, \varepsilon_{pn}) \equiv \frac{2^{3/2} I_j(\eta, \alpha, \varepsilon_{pn})}{(1+x_1)^{3/2}(1-x_1)^{\nu+1/2}} \quad (j = \sigma, E), \tag{2.8}$$

($z = 0$). Here, $I_\sigma \equiv I$ and $J_\sigma \equiv J$ are dimensionless auxiliary functions introduced and calculated in Ref. [1]; see Fig. 12 therein. Likewise, I_E and J_E are dimensionless auxiliary functions introduced and calculated in Ref. [2]; see Fig. 9 therein. The following notations have been also used:

$$\varepsilon_{\rm pn} = \frac{\varepsilon_{\rm p}}{\varepsilon_{\rm n}}, \quad x_1 = \frac{r_{\rm c}}{r}, \quad \exp\eta = \frac{1+x_1}{1-x_1}, \tag{2.9}$$

where r is the radial coordinate (Fig. 1). The quantity $v = v(\alpha, \varepsilon_{\rm pn})$ has been computed for various α and $\varepsilon_{\rm pn}$ and tabulated in Table 4 of Ref. [1].

At sufficiently long distance from the particle ($x_1 \ll 1$), Eq. (2.7) has the following asymptotic behavior [1,2]:

$$E_{\sigma,z} = -\frac{4\pi}{\varepsilon_{\rm n}}\sigma_{\rm pn}[D_3 x_1^3 + D_5 x_1^5 + O(x_1^7)], \tag{2.10}$$

$$E_{E,z} = -E_0 - E_0[H_3 x_1^3 + H_5 x_1^5 + O(x_1^7)], \tag{2.11}$$

where $D_i(\alpha, \varepsilon_{\rm pn})$ and $H_i(\alpha, \varepsilon_{\rm pn})$, $i = 3, 5$, are coefficient functions. $H_3(\alpha, \varepsilon_{\rm pn})$ and $H_5(\alpha, \varepsilon_{\rm pn})$ have been calculated in Ref. [2]. $D_3(\alpha, \varepsilon_{\rm pn})$ coincides with $D(\alpha, \varepsilon_{\rm pn})$ in Ref. [1]. In relation to the present study, we calculated also $D_5(\alpha, \varepsilon_{\rm pn})$ from the expression

$$D_5 = 2^{3/2}\int_0^\infty \frac{\tau\ \Psi_{\rm s}(\tau)}{\sinh[(\pi-\alpha)\tau]}\left(\frac{5}{4}-\tau^2\right){\rm d}\tau, \tag{2.12}$$

which has been derived completely analogously to Eq. (3.19) in Ref. [2]; τ is an integration variable. To calculate D_5, one has to substitute $\Psi_{\rm s}(\tau)$ computed as explained in Section 5.1 of Ref. [1]. For readers convenience, the functions $D_i(\alpha, \varepsilon_{\rm pn})$ and $H_i(\alpha, \varepsilon_{\rm pn})$, $i = 3, 5$, are tabulated in Tables 1–4 of Appendix A.

The numerical data in Tables 1–7 of Appendix A can be used for a fast and convenient calculation of the functions $D_i(\alpha, \varepsilon_{\rm pn})$, $H_i(\alpha, \varepsilon_{\rm pn})$, $i = 3, 5$, and other functions of α and $\varepsilon_{\rm pn}$, in the following way. Let $f(\alpha, \varepsilon_{\rm pn})$ be either of the above tabulated functions. We are interested to obtain its value for a given $\alpha_1 < \alpha < \alpha_2$, and $\varepsilon_1 < \varepsilon_{\rm pn} < \varepsilon_2$, where α_1, α_2, ε_1, and ε_2 are values given in the respective table. Then, $f(\alpha, \varepsilon_{\rm pn})$ can be calculated by means of the following four-point interpolation formula:

$$\begin{aligned} f(\alpha,\varepsilon_{\rm pn}) = {} & \frac{(\alpha-\alpha_2)(\varepsilon_{\rm pn}-\varepsilon_2)}{(\alpha_1-\alpha_2)(\varepsilon_1-\varepsilon_2)}f(\alpha_1,\varepsilon_1) \\ & + \frac{(\alpha-\alpha_2)(\varepsilon_{\rm pn}-\varepsilon_1)}{(\alpha_1-\alpha_2)(\varepsilon_2-\varepsilon_1)}f(\alpha_1,\varepsilon_2) \\ & + \frac{(\alpha-\alpha_1)(\varepsilon_{\rm pn}-\varepsilon_2)}{(\alpha_2-\alpha_1)(\varepsilon_1-\varepsilon_2)}f(\alpha_2,\varepsilon_1) \\ & + \frac{(\alpha-\alpha_1)(\varepsilon_{\rm pn}-\varepsilon_1)}{(\alpha_2-\alpha_1)(\varepsilon_2-\varepsilon_1)}f(\alpha_2,\varepsilon_2) \end{aligned} \tag{2.13}$$

As an illustration, the coefficient functions D_3 and D_5 in the multipole expansion of the electric field for charged particles, Eq. (2.10), are plotted vs. the central angle α in Fig. 1 for nine different values of $\varepsilon_{\rm pn}$. To avoid the divergence at $\alpha \to \pi$, D_3 and D_5 are scaled with powers of the factor:

$$A = \frac{2\pi\ R^2(1-\cos\alpha)}{\pi\ r_{\rm c}^2} = \frac{2}{1+\cos\alpha}. \tag{2.14}$$

A is equal to the area of $S_{\rm pn}$ divided by the area encircled by the contact line (Fig. 1). As seen in Fig. 2, the rescaled functions $D_3(\alpha, \varepsilon_{\rm pn})/A^{3/2}$ and $D_5(\alpha, \varepsilon_{\rm pn})/A^{5/2}$ have bounded variation. D_3 is positive for all $0 < \alpha < \pi$, whereas D_5 is negative for the more hydrophobic particles ($\alpha > 110°$).

The two series expansions, Eqs. (2.10) and (2.11), will be used in Section 4 to estimate the asymptotic behavior of the electrostatic interaction between two floating charged particles.

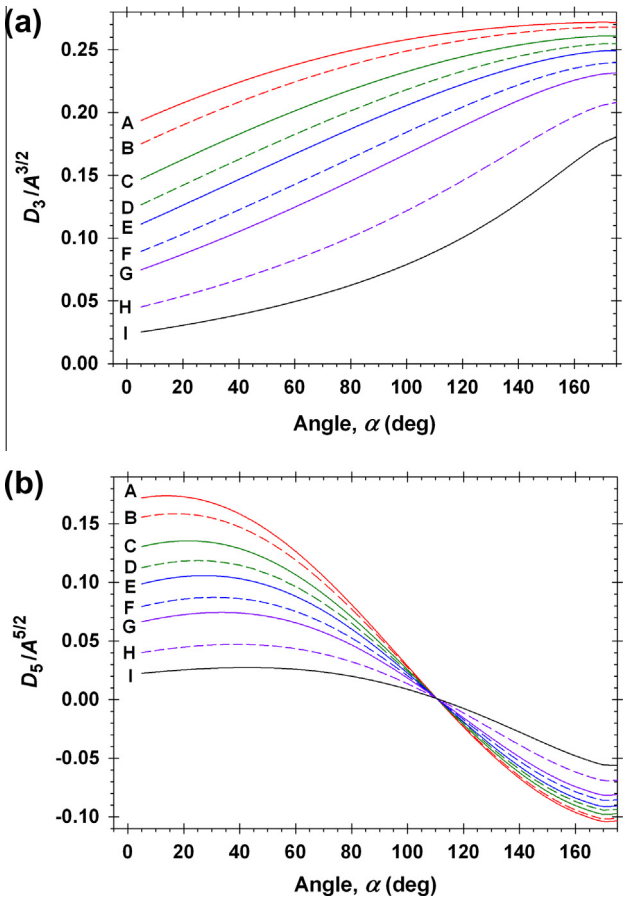

Fig. 2. Dependences of coefficient functions $D_3(\alpha, \varepsilon_{\rm pn})$ and $D_5(\alpha, \varepsilon_{\rm pn})$ on the central angle α at different fixed values of the ratio $\varepsilon_{\rm pn} = \varepsilon_{\rm p}/\varepsilon_{\rm n}$: (A) 0.125; (B) 0.250; (C) 0.500; (D) 0.750; (E) 1.00; (F) 1.50; (G) 2.00; (H) 4.00; and (I) 8.00. The scaling factor A is defined by Eq. (2.14).

3. Electrodipping force

3.1. General expressions

In the presence of electric field, the pressure is given by the Maxwell tensor $\mathbf{P}_k$ [44]:

$$\mathbf{P}_k = \left(p_{k\infty} + \frac{\varepsilon_k}{8\pi}\nabla\varphi_k\cdot\nabla\varphi_k\right)\mathbf{U} - \frac{\varepsilon_k}{4\pi}\nabla\varphi_k\nabla\varphi_k \quad (k = {\rm n}, {\rm p}, {\rm w}), \tag{3.1}$$

where $\mathbf{U}$ is the unit tensor; ∇ is the del operator; the subscripts "n", "p" and "w" denote quantities related to the nonpolar fluid, particle, and water phases; $p_{k\infty}$ is a constant scalar pressure; φ_k is electrostatic potential; and ε_k is dielectric constant. We assume that in the water phase $p_{\rm w\infty}$ is known. Far from the particle, its electric field vanishes (only E_0 remains), and the water–nonpolar interface is planar, so that the relation between $p_{\rm n\infty}$ and $p_{\rm w\infty}$ is as follows:

$$p_{\rm n\infty} - \frac{\varepsilon_{\rm n}E_0^2}{8\pi} = p_{\rm w\infty}. \tag{3.2}$$

In view of Eqs. (3.1) and (3.2), the pressure tensors in the nonpolar fluid and water phases are:

$$\mathbf{P}_{\rm n} = \left(p_{\rm w\infty} + \frac{\varepsilon_{\rm n}E_0^2}{8\pi} + \frac{\varepsilon_{\rm n}}{8\pi}\nabla\varphi_{\rm n}\cdot\nabla\varphi_{\rm n}\right)\mathbf{U} - \frac{\varepsilon_{\rm n}}{4\pi}\nabla\varphi_{\rm n}\nabla\varphi_{\rm n}, \tag{3.3}$$

$$\mathbf{P}_{\rm w} = p_{\rm w\infty}\mathbf{U}, \tag{3.4}$$

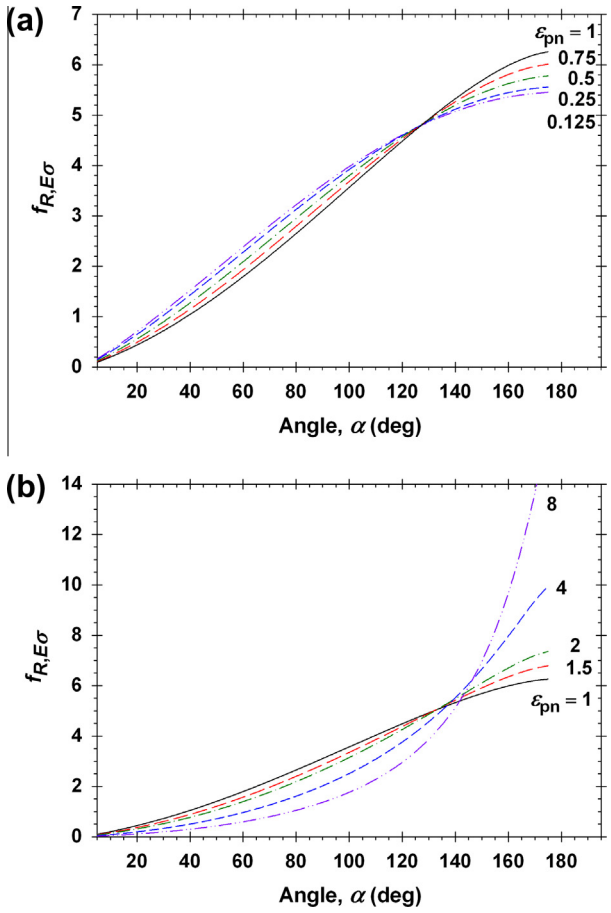

Fig. 3. Dependence of the force coefficient $f_{R,E\sigma}$ on the central angle α at different fixed values of the dielectric constant ratio $\varepsilon_{pn} = \varepsilon_p/\varepsilon_n$.

where the non-penetration of the electric field into the water phase (see Section 2.1) has been taken into account.

The electric force, **F**, acting on the particle (Fig. 1) is equal to the integral of the pressure tensor (with negative sign) over the particle surface [44]

$$\mathbf{F} = -\int_{S_{pw}} d\mathbf{S}\cdot\mathbf{P}_w - \int_{S_{pn}} d\mathbf{S}\cdot\mathbf{P}_n, \tag{3.5}$$

where d**S** is the vector surface element. From the Navier–Stokes equation, it follows that at mechanical equilibrium (in the absence of hydrodynamic flow in the two adjacent fluid phases), we can write $\nabla\cdot\mathbf{P}_n = \mathbf{0}$ and $\nabla\cdot\mathbf{P}_w = \mathbf{0}$. The integration of the latter equations over the volumes of the nonpolar fluid and water phases, V_n and V_w, and the application of the Gauss-Ostrogradsky divergence theorem yields:

$$\mathbf{0} = \int_{V_n} dV\,\nabla\cdot\mathbf{P}_n = \int_{S_{pn}} d\mathbf{S}\cdot\mathbf{P}_n + \int_{S_{nw}} dS(-\mathbf{e}_z)\cdot\mathbf{P}_n, \tag{3.6}$$

$$\mathbf{0} = \int_{V_w} dV\,\nabla\cdot\mathbf{P}_w = \int_{S_{pw}} d\mathbf{S}\cdot\mathbf{P}_w + \int_{S_{nw}} dS\mathbf{e}_z\cdot\mathbf{P}_w, \tag{3.7}$$

where dS is the scalar surface element, and $\mathbf{e}_z$ is the unit vector of the vertical z-axis. Combining Eqs. (3.3)–(3.7), we obtain:

$$\mathbf{F} = -\int_{S_{nw}} dS\mathbf{e}_z\cdot\left[\frac{\varepsilon_n}{4\pi}\nabla\varphi_n\nabla\varphi_n - \frac{\varepsilon_n}{8\pi}(\nabla\varphi_n\cdot\nabla\varphi_n + E_0^2)\mathbf{U}\right]. \tag{3.8}$$

In other words, the force **F** acting on the particle is expressed by integral over the flat nonpolar fluid–water interface, S_{nw} (Fig. 1). In accordance with Eq. (2.2), the nonpolar fluid–water interface is equipotential, $\varphi_n = 0$ at S_{nw}, and consequently, $\nabla\varphi_n = -\mathbf{e}_z E_z$ at S_{nw}. Then, Eq. (3.8) reduces to:

$$\mathbf{F} = -\mathbf{e}_z\frac{\varepsilon_n}{8\pi}\int_{S_{nw}} dS(E_z^2 - E_0^2). \tag{3.9}$$

3.2. Force coefficients

To calculate the vertical (electrodipping) force $F_z = \mathbf{e}_z\cdot\mathbf{F}$ acting on the particle (Fig. 1), we substitute Eq. (2.7) into Eq. (3.9). The result can be expressed in the form:

$$F^{(n)} \equiv F_z = -\frac{\varepsilon_n E_0^2 R^2}{4\pi} f_{R,EE} - 2E_0\sigma_{pn}R^2 f_{R,E\sigma} - \frac{4\pi\sigma_{pn}^2 R^2}{\varepsilon_n} f_{R,\sigma\sigma}, \tag{3.10}$$

where

$$f_{R,EE} = \pi\sin^2\alpha\int_0^1\left[2\left(\frac{2}{1-x_1^2}\right)^{3/2} I_E + \left(\frac{2x_1}{1-x_1^2}\right)^3 I_E^2\right]dx_1. \tag{3.11}$$

$$f_{R,\sigma\sigma} = \pi\sin^2\alpha\int_0^1\left(\frac{2x_1}{1-x_1^2}\right)^3 I_\sigma^2 dx_1. \tag{3.12}$$

$$f_{R,E\sigma} = \pi\sin^2\alpha\int_0^1\left[\left(\frac{2}{1-x_1^2}\right)^{3/2} I_\sigma + \left(\frac{2x_1}{1-x_1^2}\right)^3 I_E I_\sigma\right]dx_1. \tag{3.13}$$

The coefficient function $f_{R,EE}(\alpha, \varepsilon_{pn})$ was calculated in Ref. [2] and plotted in Fig. 10 therein. The coefficient function $f_{R,\sigma\sigma}(\alpha, \varepsilon_{pn}) \equiv f_R(\alpha, \varepsilon_{pn})$ was calculated in Ref. [1] and plotted in Fig. 11 therein.

Here, we calculate the coefficient function $f_{R,E\sigma}(\alpha, \varepsilon_{pn})$. To avoid the weak singularity of the integrand in Eq. (3.13) at $x_1 \to 1$, we split the integral in two parts:

$$\frac{f_{R,E\sigma}}{\pi\sin^2\alpha} = \int_0^{1-\delta}\left[\left(\frac{2}{1-x_1^2}\right)^{3/2} I_\sigma + \left(\frac{2x_1}{1-x_1^2}\right)^3 I_E I_\sigma\right]dx_1 + f_{\delta,E\sigma}, \tag{3.14}$$

$$f_{\delta,E\sigma} \equiv \int_{1-\delta}^1\left[\left(\frac{2}{1-x_1^2}\right)^{3/2} I_\sigma + \left(\frac{2x_1}{1-x_1^2}\right)^3 I_E I_\sigma\right]dx_1. \tag{3.15}$$

where δ is a small number; good accuracy can be obtained setting $\delta = 0.01$. The integral in Eq. (3.14) was solved numerically, calculating the functions $J_j(x_1, \alpha, \varepsilon_{pn})$, $j = E, \sigma$, as explained in Refs. [1,2]; see also Eq. (2.8). Furthermore, Eq. (3.15) can be represented in the form:

$$f_{\delta,E\sigma} \approx \int_{1-\delta}^1\left[(1-x_1)^{\nu-1}J_{\sigma 1} + (1-x_1)^{2\nu-2}J_{E1}J_{\sigma 1}\right]dx_1 = \frac{\delta^\nu}{\nu}J_{\sigma 1} + \frac{\delta^{2\nu-1}}{2\nu-1}J_{E1}J_{\sigma 1}. \tag{3.16}$$

where

$$J_{j1}(\alpha, \varepsilon_{pn}) \equiv J_j(1, \alpha, \varepsilon_{pn}) = \lim_{x_1\to 1}\left[\frac{I_j(\eta, \alpha, \varepsilon_{pn})}{(1-x_1)^{\nu+1/2}}\right], \tag{3.17}$$

$j = E, \sigma$. The function $J_{E1}(\alpha, \varepsilon_{pn})$ was calculated and tabulated in Table 2 of Ref. [2] and plotted in Fig. 8 therein. The coefficient function $J_{\sigma 1}(\alpha, \varepsilon_{pn}) \equiv C(\alpha, \varepsilon_{pn})$ was calculated and tabulated in Table 2 of Ref. [1] and plotted in Fig. 10 therein. Numerical values of $J_{E1}(\alpha, \varepsilon_{pn})$ and $J_{\sigma 1}(\alpha, \varepsilon_{pn})$ can be obtained using the respective tables along with Eq. (2.13).

The calculated dependence $f_{R,E\sigma}(\alpha, \varepsilon_{pn})$ is illustrated in Fig. 3. The latter figure shows that $f_{R,E\sigma}$ is an increasing function of α. In addition, $f_{R,E\sigma}$ is positive, so that the sign of the respective term in Eq. (3.10) is determined by the sign of the product $E_0\sigma_{pn}$. Numerical values of the coefficient functions $f_{R,EE}(\alpha, \varepsilon_{pn})$, $f_{R,\sigma\sigma}(\alpha, \varepsilon_{pn})$, and $f_{R,E\sigma}(\alpha, \varepsilon_{pn})$ can be obtained by using Tables 5–7 in Appendix A along with Eq. (2.13).

3.3. Direction of the vertical force F_z

To investigate the effect of the external electric field, E_0, on F_z, we represent Eq. (3.10) in the form:

$$F_z = -\frac{4\pi\sigma_{\rm pn}^2 R^2}{\varepsilon_{\rm n}} f_{R,EE}(N^2 + 2A_{E\sigma}N + A_{\sigma\sigma}). \tag{3.18}$$

where we have introduced the notations

$$N \equiv \frac{\varepsilon_{\rm n} E_0}{4\pi\sigma_{\rm pn}}, \tag{3.19}$$

$$A_{E\sigma} \equiv \frac{f_{R,E\sigma}}{f_{R,EE}}, \quad A_{\sigma\sigma} \equiv \frac{f_{R,\sigma\sigma}}{f_{R,EE}}. \tag{3.20}$$

The two roots of the quadratic trinomial in the parentheses in Eq. (3.18) are

$$N_{1,2} = -A_{E\sigma} \pm [(A_{E\sigma})^2 - A_{\sigma\sigma}]^{1/2}. \tag{3.21}$$

The obtained numerical results for $f_{R,EE}$, $f_{R,\sigma\sigma}$, and $f_{R,E\sigma}$ show that $(A_{E\sigma})^2 > A_{\sigma\sigma}$, i.e., the discriminant in Eq. (3.21) is always positive so that the quadratic trinomial in Eq. (3.18) has two real roots, N_1 and N_2, for $f_{R,EE} \neq 0$. In addition, Eq. (3.12) and the obtained numerical results (Fig. 3) show that $f_{R,\sigma\sigma}$ and $f_{R,E\sigma}$ are positive quantities. Hence, the sign of F_z in Eq. (3.18) is determined by $f_{R,EE}$ and N, which could take both positive and negative values. Depending on the sign of $f_{R,EE}$, the possible cases can be systematized as follows:

(a) If $f_{R,EE} > 0$ (and $A_{E\sigma} > 0$), then N_1 and N_2 in Eq. (3.21) are both negative. In this case, F_z is positive for $N_1 < N < N_2$, and negative outside this interval; see Eq. (3.18) and Fig. 4a. The three possible cases are as follows:

$$F_z > 0 \quad \text{for} \quad |N + A_{E\sigma}| < [(A_{E\sigma})^2 - A_{\sigma\sigma}]^{1/2}, \tag{3.22}$$

$$F_z < 0 \quad \text{for} \quad |N + A_{E\sigma}| > [(A_{E\sigma})^2 - A_{\sigma\sigma}]^{1/2}, \tag{3.23}$$

$$F_z = 0 \quad \text{for} \quad |N + A_{E\sigma}| = [(A_{E\sigma})^2 - A_{\sigma\sigma}]^{1/2}. \tag{3.24}$$

(b) If $f_{R,EE} < 0$ (and $A_{E\sigma} < 0$), then N_1 is negative, but N_2 is positive; see Eq. (3.21). In this case, F_z is negative for $N_1 < N < N_2$, and positive outside this interval; see Eq. (3.18) and Fig. 4b. The three possible cases are as follows:

$$F_z < 0 \quad \text{for} \quad |N + A_{E\sigma}| < [(A_{E\sigma})^2 - A_{\sigma\sigma}]^{1/2}, \tag{3.25}$$

$$F_z > 0 \quad \text{for} \quad |N + A_{E\sigma}| > [(A_{E\sigma})^2 - A_{\sigma\sigma}]^{1/2}, \tag{3.26}$$

and Eq. (3.24) holds again for the case $F_z = 0$.

(c) If $f_{R,EE} = 0$, then the term with N^2 in Eq. (3.18) disappears and F_z depends linearly on N; see Fig. 4c. The three possible cases are as follows:

$$F_z > 0 \quad \text{for} \quad N < N_0, \tag{3.27}$$

$$F_z < 0 \quad \text{for} \quad N > N_0, \tag{3.28}$$

$$F_z = 0 \quad \text{for} \quad N = N_0, \tag{3.29}$$

where

$$N_0 \equiv -\frac{f_{R,\sigma\sigma}}{2f_{R,E\sigma}} < 0. \tag{3.30}$$

Because $N \propto E_0$, see Eq. (3.19), the above results indicate that for all values of the contact angle, α, and of the dielectric constant ratio, $\varepsilon_{\rm pn} = \varepsilon_{\rm p}/\varepsilon_{\rm n}$, the direction and magnitude of F_z can be controlled using the external electric field E_0.

3.4. Numerical results for F_z

Fig. 5 illustrates the sign and magnitude of F_z depending on the applied external electric field E_0 for a hydrophilic particle with $\alpha = 60°$ (Fig. 5a) and for a hydrophobic particle with $\alpha = 120°$ (Fig. 5b). In view of Eq. (3.18), it is convenient to plot the dimensionless force,

$$F_{z,\rm d} \equiv \frac{\varepsilon_{\rm n} F_z}{4\pi\sigma_{\rm pn}^2 R^2}, \tag{3.31}$$

vs the dimensionless electric field $E_{0,\rm d} \equiv N$; see Eq. (3.19).

In accordance with Eq. (3.18), the $F_{z,\rm d}$-vs.-$E_{0,\rm d}$ curves in Fig. 5 are parabolas. At $E_{0,\rm d} = 0$, in all cases $F_{z,\rm d} < 0$, which is the electrodipping force solely due to the effect of the particle surface charge, $\sigma_{\rm pn}$, viz. $F_{z,\rm d}|_{E_0=0} = -f_{R,\sigma\sigma}$. The latter force is relatively small by magnitude as compared to the effect that can be produced by the external electric field $E_{0,\rm d}$; see Fig. 5.

In addition, it turns out that $(A_{E\sigma})^2 \gg A_{\sigma\sigma}$. Thus, expanding in series under the square root in Eq. (3.21), we obtain that one of the roots N_1 and N_2, which is smaller by magnitude, is close to N_0 in Eq. (3.30). For this reason, all curves in Fig. 5 are close to each other at $E_{0,\rm d} \approx N_0$.

For hydrophilic particles with $\alpha = 60°$ (Fig. 5a), at $\varepsilon_{\rm pn} < 4$ we have $f_{R,EE} > 0$, and the $F_{z,\rm d}$-vs.-$E_{0,\rm d}$ curves resemble that in Fig. 4a. In this case, $F_{z,\rm d}$ tends to deep the particles into the water phase, except in the region $N_1 < E_{0,\rm d} < N_2$, where the external field pulls the particle toward the nonpolar fluid. The latter corresponds to an oppositely charged electrode placed in the nonpolar fluid, which attracts the particle. Note, however, that at $E_{0,\rm d} < N_1$, again for oppositely charged particle and electrode, F_z changes sign and pushes the particles into the water. This is due to the predominant effect of particle polarization, expressed by the term $\propto f_{R,EE}N^2$ in Eq. (3.18), that overcomes the effect of $\sigma_{\rm pn}$.

In Fig. 5a, $f_{R,EE}$ changes sign at $\varepsilon_{\rm pn} \approx 4$, where the plot of $F_{z,\rm d}$ vs. $E_{0,\rm d}$ resembles that in Fig. 4c. At $\varepsilon_{\rm pn} = 8$, the pulling-up effect of the term $f_{R,EE}N^2$ is predominant, except in the interval region $N_1 < E_{0,\rm d} < N_2$, where the effect of the particle charge $\sigma_{\rm pn}$ gets the upper hand.

At $\alpha = 120°$ in Fig. 5b, all effects are similar, the main difference being that the pull-up effects are predominant, which is due to the smaller (more negative) values of $f_{R,EE}$ at this contact angle that lead to a situation like that in Fig. 4b; see also Fig. 10 in Ref. [2].

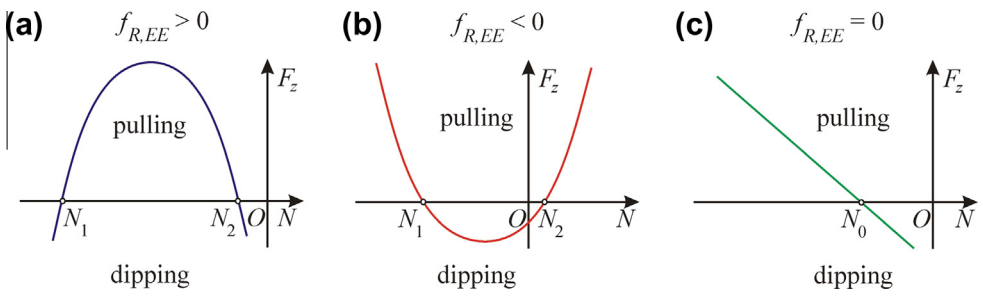

Fig. 4. On the determination of the sign of the normal electric force F_z depending on the dimensionless number N in Eq. (3.18): (a) for $f_{R,EE} > 0$; (b) for $f_{R,EE} < 0$ and (c) for $f_{R,EE} = 0$.

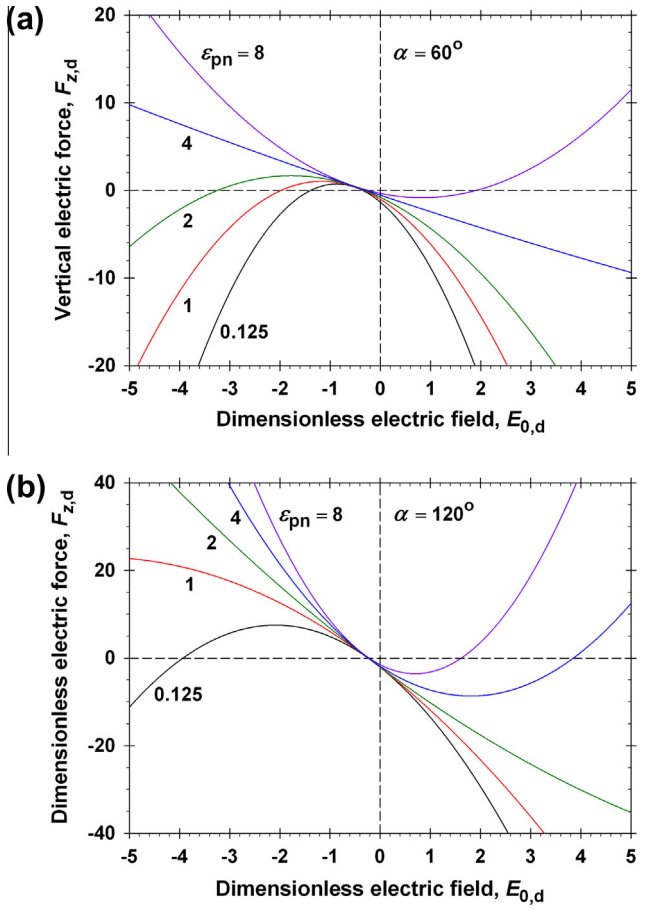

Fig. 5. Plot of the dimensionless normal (electrodipping) force, $F_{z,d}$, vs. the dimensionless external electric field, $E_{0,d} \equiv N$; see Eqs. (3.19) and (3.31) for their definitions. Each curve is a parabola that has two zeros, except that with $f_{R,EE} = 0$ (corresponding to a certain $\varepsilon_{pn} = \varepsilon_p/\varepsilon_n$), for which the plot is a straight line; see Eq. (3.18) and Fig. 4.

4. Lateral electric force between two particles at the interface

4.1. Theoretical expression for the lateral force

Here, we are using the solution of the single-particle problem to derive an expression for the force of electrostatic interaction between two identical charged particles attached to the water–nonpolar fluid interface. The particles are separated at a distance L between the centers of their contact lines (Fig. 6). As before, an external electric field $\mathbf{E}_0$ is applied normal to the fluid interface. The electrostatic interaction between the particles is due to both their surface charges and their polarization by the external field.

Substituting Eqs. (3.3) and (3.4) into Eq. (3.5), we obtain the following general expression for the electric force acting on a given particle:

$$\mathbf{F} = \int_{S_{pn}} \left[\frac{\varepsilon_n}{4\pi}\nabla\varphi_n\nabla\varphi_n - \frac{\varepsilon_n}{8\pi}(\nabla\varphi_n\cdot\nabla\varphi_n + E_0^2)\mathbf{U}\right]\cdot d\mathbf{S}. \tag{4.1}$$

Furthermore, let us construct an imaginary rectangular parallelepiped around one of the two particles, as depicted in Fig. 6. The lower base $A_1A_2A_3A_4$ lies on the water–nonpolar fluid interface. The right side of the parallelepiped, $A_1A_2B_2B_1$, is located in the middle between the particles and coincides with the yz-plane of the Cartesian coordinate system (Fig. 6).

As in Section 3.1, we can take a volume integral of the equilibrium relation $\nabla\cdot\mathbf{P}_n = \mathbf{0}$, and use the Gauss-Ostrogradsky divergence

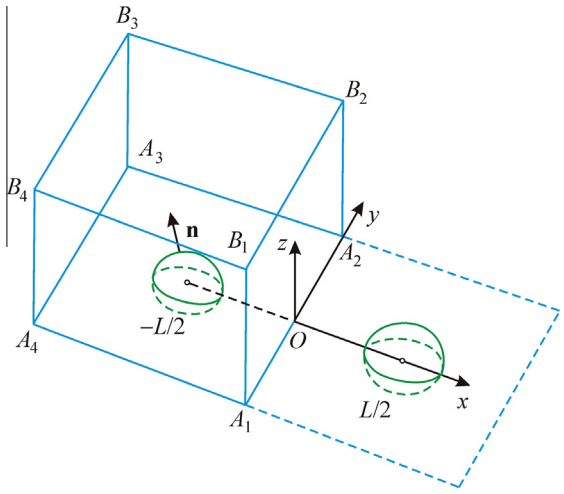

Fig. 6. Imaginary parallelepiped used for the derivation of the expression for the force between two identical charged particles at the water–nonpolar fluid interface; L is the interparticle center-to-center distance (details in the text).

theorem. As a result, the integral in Eq. (4.1) over the upper portion of the particle surface, S_{pn}, is transformed into sums of integrals over the sides of the considered parallelepiped. Thus, from Eq. (4.1), we obtain the following expression for the x-projection of the repulsive force acting on the left-hand-side particle:

$$\begin{aligned} F_{12} \equiv F_x^{(el)} &= -\int_{A_1A_2B_2B_1}\left[\frac{\varepsilon_n}{4\pi}\left(\frac{\partial\varphi_n}{\partial x}\right)^2 - \frac{\varepsilon_n}{8\pi}(\nabla\varphi_n\cdot\nabla\varphi_n + E_0^2)\right]dS \\ &+ \int_{A_4A_3B_3B_4}\left[\frac{\varepsilon_n}{4\pi}\left(\frac{\partial\varphi_n}{\partial x}\right)^2 - \frac{\varepsilon_n}{8\pi}(\nabla\varphi_n\cdot\nabla\varphi_n + E_0^2)\right]dS \end{aligned} \tag{4.2}$$

In Eq. (4.2), only the integrals over the right and left sides of the parallelepiped have remained. The integrals over the other sides give zero contributions because of the following reasons. The integrals over the front and back sides, $A_1B_1B_4A_4$ and $A_2B_2B_3A_3$, cancel each other because of the symmetry. The integral over the lower base is zero because of the boundary condition $\varphi_n = 0$ at S_{nw}, see Eq. (2.2). The integral over the upper base $B_1B_2B_3B_4$ vanishes because it is assumed that this side is situated far from the particle. For the same reason, $\varphi_n = E_0 z$ over the left side $A_4A_3B_3B_4$, so that the second integral in Eq. (4.2) can be considerably simplified. The respective integration limits can be set at infinity, and the integral in Eq. (4.2) acquires the form:

$$F_x^{(el)} = \frac{\varepsilon_n}{8\pi}\int_{-\infty}^{\infty}dy\int_0^{\infty}dz\left[\left(\frac{\partial\varphi_n}{\partial y}\right)^2 + \left(\frac{\partial\varphi_n}{\partial z}\right)^2 - E_0^2)\right] \quad \text{at } x = 0. \tag{4.3}$$

Note that because of the symmetry of the system, φ^n has extremum in the middle between the two identical particles and consequently $\partial\varphi^n/\partial x = 0$ over the midplane. Next, φ^n can be expressed as a sum of a contribution $E^0 z$ from the external field and of the potential $\tilde{\varphi}_n$ due to the particles:

$$\varphi_n \equiv E_0 z + \tilde{\varphi}_n, \tag{4.4}$$

The substitution of Eq. (4.4) into Eq. (4.3) yields:

$$F_x^{(el)} = \frac{\varepsilon_n}{8\pi}\int_{-\infty}^{\infty}dy\int_0^{\infty}dz\left[\left(\frac{\partial\tilde{\varphi}_n}{\partial y}\right)^2 + \left(\frac{\partial\tilde{\varphi}_n}{\partial z}\right)^2 + 2E_0\frac{\partial\tilde{\varphi}_n}{\partial z}\right] \quad \text{at } x = 0. \tag{4.5}$$

The integral of the last term in the brackets gives zero, because $\tilde{\varphi}_n|_{z=0} = \tilde{\varphi}_n|_{z\to\infty} = 0$. Thus, Eq. (4.5) acquires a simpler form:

$$F_x^{(el)} = \frac{\varepsilon_n}{8\pi}\int_{-\infty}^{\infty} dy \int_0^{\infty} dz \left[\left(\frac{\partial\tilde{\varphi}_n}{\partial y}\right)^2 + \left(\frac{\partial\tilde{\varphi}_n}{\partial z}\right)^2\right] \quad \text{at } x = 0. \tag{4.6}$$

Eq. (4.6) shows that the force of electrostatic interaction between two identical floating particles is always repulsive.

4.2. Multipole expansion

At larger distances between the particles, the electric potential $\tilde{\varphi}_n$ at the midplane can be presented as a superposition of the electric potentials $\tilde{\varphi}_{n,A}$ and $\tilde{\varphi}_{n,B}$ created by the individual particle:

$$\tilde{\varphi}_n \approx \tilde{\varphi}_{n,A} + \tilde{\varphi}_{n,B}. \tag{4.7}$$

The subscripts A and B denote quantities related, respectively, to the left- and right-hand-side particle. In view of the asymptotic expansions, Eqs. (2.10) and (2.11), we can represent Eq. (4.7) in the form:

$$\tilde{\varphi}_{n,k} = \frac{p_d}{\varepsilon_n}\frac{z}{(r_k^2+z^2)^{3/2}} + \frac{p_o}{\varepsilon_n}\left[\frac{z}{(r_k^2+z^2)^{5/2}} - \frac{5z^3}{3(r_k^2+z^2)^{7/2}}\right] \tag{4.8}$$
$$(k = A, B).$$

where the first term arises from the Legendre polynomial P_1 (dipolar term) and the second one from the Legendre polynomial P_3 (octupolar term) [46]; the dipolar and octupolar moments, p_d and p_o, are defined as follows:

$$p_d \equiv 4\pi\sigma_{pn}(D_3 + NH_3)r_c^3 \tag{4.9}$$

$$p_o \equiv 4\pi\sigma_{pn}(D_5 + NH_5)r_c^5 \tag{4.10}$$

where N is defined by Eq. (3.19); $D_i(\alpha, \varepsilon_{pn})$ and $H_i(\alpha, \varepsilon_{pn})$, $i = 3, 5$, are the coefficient functions in Eqs. (2.10) and (2.11), which are tabulated in Tables 1–4; see Appendix A and Eq. (2.13). The radial distances r_A and r_B in Eq. (4.8) are defined by the relationships

$$r_A^2 \equiv \left(x + \frac{L}{2}\right)^2 + y^2 \text{ and } r_B^2 \equiv \left(x - \frac{L}{2}\right)^2 + y^2. \tag{4.11}$$

The substitution of Eqs. (4.7), (4.8), and (4.11) in Eq. (4.6) yields:

$$F_x^{(el)} \approx -\frac{1}{32\pi\varepsilon_n}\int_{-\infty}^{\infty}\int_0^{\infty} U_x(y,z)dz\, dy, \tag{4.12}$$

where U_x is given by the expression:

$$U_x(y,z) \equiv \Big\{16y^2z^2[9p_d(L^2+4y^2+4z^2)^2 + 20p_o(3L^2+12y^2-16z^2)]^2 + [3p_d(L^2+4y^2+4z^2)^2(L^2+4y^2-8z^2) + 4p_o(3L^4+24L^2y^2 - 96L^2z^2 + 48y^4 - 384y^2z^2 + 128z^4)]^2\Big\}\frac{1}{9(L^2+4y^2+4z^2)^9}. \tag{4.13}$$

The integral in Eq. (4.12) can be taken analytically; the final result is:

$$F_x^{(el)} \approx \frac{1}{\varepsilon_n L^4}\left(\frac{3}{2}p_d^2 + \frac{5p_dp_o}{L^2} + \frac{175p_o^2}{18L^4}\right). \tag{4.14}$$

For $p_d \neq 0$, the dipolar term is predominant and then the long-distance asymptotics of the electrostatic interaction force is:

$$F_x^{(el)} \approx \frac{3p_d^2}{2\varepsilon_n L^4}. \tag{4.15}$$

where p_d is defined by Eq. (4.9).

For a special choice of the external field, $E_{0,d} \equiv N = -D_3/H_3$, we have $p_d = 0$; see Eqs. (3.19) and (4.9). In such a case, the octupolar term becomes the leading term in Eq. (4.14), so that the interaction force becomes:

$$F_x^{(el)} \approx \frac{175p_o^2}{18\varepsilon_n L^8}. \tag{4.16}$$

In the latter case, the direct electrostatic repulsion, $F_x^{(el)} \propto 1/L^8$, decays much faster than the electrocapillary attraction, $F_x^{(EC)} \propto 1/L^4$ [27,47,48], and then the net force becomes attractive at long distances.

At $p_d \neq 0$, if the exact method of reflections [49] is used [instead of the superposition approximation, Eq. (4.7)] an additional octupolar term $\propto p_d^2/L^8$ will appear in Eq. (4.14). However, for $p_d \neq 0$, the octupolar terms are negligible and the asymptotic force is given by Eq. (4.15). Conversely, if $p_d = 0$ the term $\propto p_d^2/L^8$ disappears, and the leading term is the octupolar term given by Eq. (4.16).

4.3. Numerical results and discussion

To compute $F_x^{(el)}$ for various E_0, α and ε_{pn}, we used Eqs. (4.9), (4.10), and (4.14). The coefficient functions $D_i(\alpha, \varepsilon_{pn})$ and $H_i(\alpha, \varepsilon_{pn})$, $i = 3, 5$, were calculated as explained after Eq. (2.11). In view of Eqs. (4.9), (4.10), and (4.14), it is convenient to plot the dimensionless force,

$$F_{x,d}^{(el)} \equiv \frac{\varepsilon_n F_x^{(el)}}{4\pi\sigma_{pn}^2 R^2}, \tag{4.17}$$

vs the dimensionless electric field $E_{0,d} \equiv N$; see Eq. (3.19). For the dielectric constants, we used experimental values for tetradecane and glass particles from Ref. [38], viz. $\varepsilon_n = 2.04$ and $\varepsilon_p = 3.97$. Note that by definition $r_c = R \sin\alpha$ (Fig. 1).

Fig. 7 shows plots of $F_{x,d}^{(el)}$ vs. $E_{0,d}$, calculated for seven different values of the central angle, α, at a fixed interparticle distance $L = 6R$. Because of the large variations of $F_{x,d}^{(el)}$, this quantity is plotted in logarithmic scale. For each value of α, the respective curve in Fig. 7 has a minimum. This minimum corresponds to the special value of E_0, for which the total dipole moment p_d is zero, so that the force of interaction between the two particles, $F_{x,d}^{(el)}$, is dominated by the octupolar moment, p_o; see Eq. (4.14). At $\alpha = 55°$, the minimum is located at $E_{0,d} < -30$, and for this reason, it is not visible in the figure.

The diminishing of $F_{x,d}^{(el)}$ with the decrease in α (Fig. 7) is partially due to the fact that the external electric field, which polarizes the dielectric particle, enters the particle through the surface S_{pn} (Fig. 1), but S_{pn} considerably decreases with the decrease in α.

Fig. 8 shows $F_{x,d}^{(el)}$ vs. the dimensionless distance L/R at $\alpha = 90°$, and at five different fixed values of the dimensionless electric field, $E_{0,d}$. One of them, $E_{0,d} = 3.078$, corresponds to the minimum of the dependence of $F_{x,d}^{(el)}$ on $E_{0,d}$, which is shown in the inset of Fig. 8. At

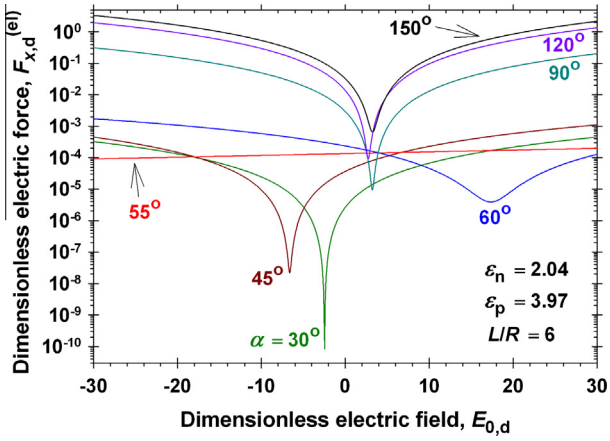

Fig. 7. Plots of the dimensionless interaction force $F_{x,d}^{(el)}$ vs. the dimensionless external electric field, $E_{0,d} \equiv N$, defined by Eqs. (3.19) and (4.17), at different fixed values of the particle contact angle, α, and at a distance $L = 6R$. The minimum of each curve corresponds to that value of $E_{0,d}$, at which the dipole moment $p_d = 0$, so that the force is determined by the octupolar moment, p_o.

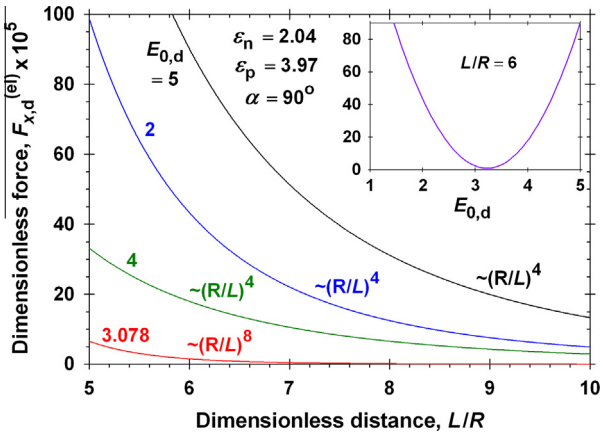

Fig. 8. Plots of the dimensionless interaction force $F_{x,d}^{(el)}$ vs. the dimensionless distance L/R at four different values of the external electric field, $E_{0,d} \equiv N$. The inset shows $F_{x,d}^{(el)}$ vs. $E_{0,d} \equiv$ at $L/R = 6$. At $E_{0,d} = 3.078$, the dipolar term in particle electric field is zero, and the interaction is dominated by the octupolar term. In this case, the electric repulsion decays much faster.

$E_{0,d} = 3.078$, the dipolar term is zero ($p_d = 0$) and we are dealing with octupole–octupole interaction, $F_x^{(el)} \propto /L^{-8}$; see Eq. (4.16). In this case, the attractive electrocapillary force $F_x^{(EC)} \propto 1/L^4$ [27,47,48] dominates the interparticle force, at least at long distances.

It should be noted also that the minima of the curves in Fig. 7 look sharp because of the used log scale. In a linear scale, all of them are rounded parabolas as the curve at $\alpha = 90°$ shown in the inset of Fig. 8.

5. Conclusions

In this study, we address the problem for calculating the electric forces acting on charged dielectric colloidal particles, which are attached to the interface between a nonpolar fluid (air and oil) and water, in the presence of applied uniform external electric field. The latter is assumed to be perpendicular to the liquid interface with vertical projection E_0. In addition, charges of surface density σ_{pn} are located on the particle–nonpolar fluid interface. We consider the case of not-too-small particles, for which the particle radius is much greater than the Debye screening length in the water phase, $\kappa R \gg 1$. In such a case, the electrostatic interactions across the water phase are negligible and only the electric effects in the nonpolar fluid and inside the dielectric particle are essential. The importance of the problem is related to the use of external electric field for controlling the distances between particles in non-densely packed interfacial colloidal crystals for producing lithographic masks with various technological applications [16–22].

The solution of the problem represents a superposition of the solutions to two simpler problems. The first one is to find the electric field due to the particle surface charges, σ_{pn}, in the absence of external field ($E_0 = 0$), which was solved in Ref. [1]. The second problem is to determine the electric field due to the polarization of an uncharged particle ($\sigma_{pn} = 0$) in the applied external field, E_0, which was solved in Ref. [2]. The combination of these solutions is non-trivial because the electric forces acting on the particle are quadratic with respect to the electric field, so that cross terms appear. General expressions are derived for calculating the normal (electrodipping) force F_z acting on each separate particle, Eq. (3.9), and the force $F_x^{(el)}$ of electrostatic interaction between two identical particles, see Eq. (4.6).

Because the uniform external field can be directed upward or downward, the effect of E_0 on F_z can have the same or the opposite direction to the effect of the particle charge, σ_{pn}. In general, the dependence of F_z on E_0 is non-monotonic and may have a maximum or minimum. The force F_z can be positive (pulling) or negative (dipping) depending on the particle contact angle and dielectric constant (see Figs. 4 and 5).

In contrast, the lateral electric force between two identical particles, $F_x^{(el)}$, cannot change sign – it is always repulsive, but it can vary by many orders of magnitude. This is because the dipolar electric field created by the particle depends on E_0 in such a way that the net dipolar moment of the particle can become zero at a given E_0. Then, the interparticle force is determined by the particle octupolar moment, which leads to a much weaker and short-range repulsion. For this reason, $F_x^{(el)}$ has a sharp minimum at the respective value of E_0 (Fig. 7). In the vicinity of this minimum, $F_x^{(el)}$ is very sensitive to the variations in E_0. This effect can be used for a fine control of the lattice spacing in non-densely packed interfacial colloidal crystal by varying the external field. The weak repulsive electric force governed by the octupolar term can be overcome by the attractive lateral capillary forces and van der Waals forces, which would lead to two-dimensional particle coagulation on the liquid interface. In contrast, if the dipolar term in the particle electric field is not eliminated by the adjustment of E_0, the electrostatic repulsion between the particles can prevent their surface coagulation and stabilize non-densely packed colloidal arrays of regular hexagonal packing [9–16].

Acknowledgments

The authors gratefully acknowledge the support from the National Science Fund of Bulgaria, Grant No. DO-02-121/2009; from the FP7 project Beyond-Everest, and from the ESF COST Action CM1101.

Appendix A. Supplementary material

Supplementary data associated with this article can be found, in the online version, at http://dx.doi.org/10.1016/j.jcis.2013.05.015.

References

[1] K.D. Danov, P.A. Kralchevsky, J. Colloid Interface Sci. 298 (2006) 213–231.
[2] K.D. Danov, P.A. Kralchevsky, J. Colloid Interface Sci. 405 (2013) 278–290.
[3] N. Aubry, P. Singh, Phys. Rev. E 77 (2008) 056302.
[4] N. Aubry, P. Singh, M. Janjua, S. Nudurupati, Proc. Natl. Acad. Sci. USA 105 (2008) 3711–3714.
[5] M. Janjua, S. Nudurupati, P. Singh, N. Aubry, Mech. Res. Commun. 36 (2009) 55–64.
[6] P. Singh, D.D. Joseph, N. Aubry, Soft Matter 6 (2010) 4310–4325.
[7] P. Singh, M. Hossain, B. Dalal, S.K. Gurupatham, I.S. Fischer, Mech. Res. Commun. 45 (2012) 54–57.
[8] K. Masschaele, J. Vermant, Soft Matter 7 (2011) 10597–10600.
[9] R. Aveyard, J.H. Clint, D. Nees, V.N. Paunov, Langmuir 16 (2000) 1969–1979.
[10] R. Aveyard, B.P. Binks, J.H. Clint, P.D.I. Fletcher, T.S. Horozov, B. Neumann, V.N. Paunov, et al., Phys. Rev. Lett. 88 (2002) 246102.
[11] T.S. Horozov, R. Aveyard, J.H. Clint, B.P. Binks, Langmuir 19 (2003) 2822–2829.
[12] E.J. Stancik, M. Kouhkan, G.G. Fuller, Langmuir 20 (2004) 90–94.
[13] R. Reynaert, P. Moldenaers, J. Vermant, Langmuir 22 (2006) 4936–4945.
[14] M.E. Leunissen, J. Zwanikken, R. van Roij, P.M. Chaikin, A. van Blaaderen, Phys. Chem. Chem. Phys. 9 (2007) 6405–6414.
[15] L. Isa, K. Kumar, M. Müller, J. Grolig, M. Textor, E. Reimhult, ACS Nano 4 (2010) 5665–5670.
[16] M.A. Ray, L. Jia, Adv. Mater. 19 (2007) 2020–2022.
[17] M.A. Ray, N. Shewmon, S. Bhawalkar, L. Jia, Y. Yang, E.S. Daniels, Langmuir 25 (2009) 7265–7270.
[18] Y. Zhao, J. Wang, G. Mao, Opt. Lett. 30 (2005) 1885–1887.
[19] W.-L. Min, P. Jiang, B. Jiang, Nanotechnology 19 (2008) 475604.
[20] A. Büttner, U.D. Zeitner, Opt. Eng. 41 (2002) 2393–2401.
[21] H. Urey, K.D. Powell, Appl. Opt. 44 (2005) 4930–4936.
[22] Y. Sun, S.R. Forrest, J. Appl. Phys. 100 (2006) 073106.
[23] D.Y.C. Chan, J.D. Henry, L.R. White, J. Colloid Interface Sci. 79 (1981) 410–418.
[24] P.A. Kralchevsky, K. Nagayama, Langmuir 10 (1994) 23–36.

[25] P.A. Kralchevsky, N.D. Denkov, Curr. Opin. Colloid Interface Sci. 6 (2001) 383–401.
[26] N.D. Vassileva, D. van den Ende, F. Mugele, J. Mellema, Langmuir 21 (2005) 11190–11200.
[27] K.D. Danov, P.A. Kralchevsky, J. Colloid Interface Sci. 345 (2010) 505–514.
[28] C. Pozrikidis, Eng. Anal. Bound. Elem. 36 (2012) 836–844.
[29] D. Stamou, C. Duschl, D. Johannsmann, Phys. Rev. E 62 (2000) 5263–5272.
[30] P.A. Kralchevsky, N.D. Denkov, K.D. Danov, Langmuir 17 (2001) 7694–7705.
[31] T.S. Horozov, R. Aveyard, B.P. Binks, J.H. Clint, Langmuir 21 (2005) 7405–7412.
[32] T.S. Horozov, B.P. Binks, Colloids Surf., A 267 (2005) 64–73.
[33] K.D. Danov, P.A. Kralchevsky, B.N. Naydenov, G. Brenn, J. Colloid Interface Sci. 287 (2005) 121–134.
[34] E.P. Lewandowski, J.A. Bernate, P.C. Searson, K.J. Stebe, Langmuir 24 (2008) 9302–9307.
[35] E.P. Lewandowski, M. Cavallaro, L. Botto, J.C. Bernate, V. Garbin, K.J. Stebe, Langmuir 26 (2010) 15142–15154.
[36] K.D. Danov, P.A. Kralchevsky, Adv. Colloid Interface Sci. 154 (2010) 91–103.
[37] C. Monteux, E. Jung, G.G. Fuller, Langmuir 23 (2007) 3975–3980.
[38] K.D. Danov, P.A. Kralchevsky, M.P. Boneva, Langmuir 20 (2004) 6139–6151.
[39] M.P. Boneva, K.D. Danov, N.C. Christov, P.A. Kralchevsky, Langmuir 25 (2009) 9129–9139.
[40] V.N. Paunov, Colloid Polym. Sci. 281 (2003) 701–707.
[41] D. Frydel, S. Dietrich, Phys. Rev. Lett. 99 (2007) 118302.
[42] A. Domínguez, D. Frydel, M. Oettel, Phys. Rev. E 77 (2008). 020401(R).
[43] A. Shrestha, K. Bohinc, S. May, Langmuir 28 (2012) 14301–14307.
[44] L.D. Landau, E.M. Lifshitz, Electrodynamics of Continuous Media, Course of Theoretical Physics, vol. 8, Pergamon Press, Oxford, 1960.
[45] K.D. Danov, P.A. Kralchevsky, K.P. Ananthapadmanabhan, A. Lips, Langmuir 22 (2006) 106–115.
[46] T.B. Jones, Electromechanics of Particles, Cambridge University Press, Cambridge, UK, 1995.
[47] A. Würger, L. Foret, J. Phys. Chem. B 109 (2005) 16435–16438.
[48] A. Domínguez, M. Oettel, S. Dietrich, J. Chem. Phys. 127 (2007) 204706.
[49] J. Happel, H. Brenner, Low Reynolds Number Hydrodynamics, Kluwer, Boston, 1983.